Noise Amplification Effects due to Jet-Surface Interaction

Falcão Loureiro Rêgo, Leandro; Avallone, Francesco; Ragni, Daniele; Casalino, Damiano

Important note
To cite this publication, please use the final published version (if applicable).
Please check the document version above.

Noise Amplification Effects due to Jet-Surface Interaction

Leandro Rego*, Francesco Avallone†, Daniele Ragni‡ and Damiano Casalino§
Delft University of Technology, Delft, 2629HS, The Netherlands

A numerical investigation on jet-installation noise is performed using a software based on the Lattice-Boltzmann Method. A flat plate is placed in the irrotational hydrodynamic field of the jet, i.e. outside of the plume, resulting in noise increase due to the scattering of instability waves at the plate trailing edge. The configuration adopted in this work replicates the one used for a benchmark study at NASA Glenn, against which the numerical results are validated. Far-field noise spectra from the isolated and installed jet cases, obtained through the Ffowcs-Williams Hawkings analogy, are compared at different polar angles. The results show a low-frequency noise amplification, occurring mainly in the directions normal to the plate and upstream of the jet axis. It is also shown that strong pressure fluctuations are generated at the trailing-edge of the plate and then propagate to the far-field as acoustic waves. The effects of the plate geometry (length and radial position) and jet flow characteristics (velocity and temperature) on the installation noise are also addressed. Pressure fluctuations on the plate are also computed and correlated to the overall far-field results, showing that, in the installed case, the surface dipoles are the dominant sources at low frequencies.

Nomenclature

c_0	=	ambient speed of sound [m/s]
D_j	=	nozzle exit diameter [mm]
f	=	frequency [Hz]
h	=	radial distance between the flat plate and the jet centerline [mm]
L	=	flat plate trailing-edge axial position [mm]
M	=	Mach number
M_a	=	acoustic Mach number (U_j/c_0)
NPR	=	nozzle pressure ratio relative to the ambient conditions
Re	=	Reynolds number
St	=	Strouhal number
T_R	=	temperature ratio between the jet and ambient conditions
u	=	velocity component in the $x-$direction [m/s]
u'	=	velocity fluctuations in the $x-$direction [m/s]
U_j	=	nominal jet velocity [m/s]
ϕ	=	azimuthal angle of the observer [°]
θ	=	polar angle of the observer [°]

I. Introduction

THE high bypass ratio of current turbofans results in significant benefits in terms of fuel burn and jet noise reductions due to lower exhaust flow velocities [1]. Consequently, the engine diameters become larger, which requires them to be mounted closer to the wing in order to maintain a minimum ground clearance. This results in an interaction between the jet and a nearby airframe surface, generating an additional source known as jet-installation noise (JIN) [2]. The JIN is especially significant during take-off and approach flight conditions, when the deployed high-lift systems are positioned close to the jet plume [3], with significant noise increase at low and mid-frequencies [4, 5]. Therefore, the

---
*PhD Candidate, Aerodynamics, Wind Energy, Flight Performance and Propulsion Department, l.rego@tudelft.nl, AIAA Student Member
†Assistant Professor, Aerodynamics, Wind Energy, Flight Performance and Propulsion Department, f.avallone@tudelft.nl
‡Assistant Professor, Aerodynamics, Wind Energy, Flight Performance and Propulsion Department, d.ragni@tudelft.nl
§Professor, Aerodynamics, Wind Energy, Flight Performance and Propulsion Department, d.casalino@tudelft.nl

characteristics of the phenomena behind engine installation effects, such as the relationship between the near-field properties of the jet and the far-field noise, must be fully understood so that appropriate noise reduction solutions can be developed, and posteriorly applied on aircraft.

The noise generation mechanism due to the interaction between a jet and a nearby infinite solid boundary was firstly addressed by Curle [6]. Curle's formulation states that the hydrodynamic perturbations from the jet impinge on a surface, producing pressure fluctuations. The resulting sound field is then equivalent to a distribution of acoustic dipoles. Therefore, at low Mach numbers, the noise produced by those fluctuations is more acoustically efficient than that produced by free turbulence [6]. For the case of a semi-infinite surface interacting with a jet, it was demonstrated by Ffowcs-Williams and Hall that the trailing-edge of the suface scatters the pressure fluctuations from the jet as sound to the far-field [7]. The sound intensity produced by this source was found to be proportional to the fifth power of the velocity, and thus it is likely the most efficient noise generation mechanism for this configuration, at low Mach numbers.

An isolated subsonic jet displays a broadband noise spectrum with a superdirective characteristic, i.e. by approaching polar angles in the direction of the jet axis, an exponential increase in noise occurs, which is dominated by the axisymmetric azimuthal mode of the sound field [8]. For an installed jet, it has been shown that the scattering effects usually occur at low and mid frequencies, followed by either reflection or shielding of acoustic waves at higher frequencies [9]. The sound directivity patterns are consistent with dipole sources: in the azimuthal direction, there are two lobes with peaks in the directions normal to the surface, whereas in the surface plane there is no noise increase. In the polar direction, a cardioid pattern is obtained, with the maximum amplification in the upstream direction of the jet. At low polar angles, towards the jet axis in the downstream direction, noise levels similar to the ones of the isolated configuration are found [9].

The characteristics of the JIN are dependent on the geometry of the surface, namely its length and position relative to the jet axis [10, 11]. If the surface is placed in the jet acoustic field, far enough from the plume, where convective terms can be neglected, only scattering of acoustic waves will occur and there will be no significant changes to the overall noise [11]. However, if the surface is placed in the irrotational region of the jet hydrodynamic field, the trailing-edge scattering of impinging pressure waves is responsible for a large sound amplification [11, 12]. Finally, if the surface is placed inside the rotational jet flow, the consequent grazing on the plate will result in the formation of a boundary layer, and thus, there will be an additional component of trailing-edge noise [13].

This work aims to provide an assessment of the jet-installation noise phenomena via numerical calculations performed with the Lattice-Boltzmann Method (LBM). One of the advantages of the LBM is that high-fidelity simulations can be carried out with the actual geometry of interest. Highly accurate results can obtained, when compared to experimental data, as shown by van der Velden et al. [14], for the case of an isolated jet. The installed jet configuration selected for this work replicates the one from the jet-surface interaction benchmark study performed at NASA Glenn, with a single-stream nozzle and a nearby flat plate [15, 16]. This model is appropriate for more fundamental analyses, with low computational costs, while still displaying the main characteristics of the JIN.

This paper is organized as follows. The model configuration is described in Section II, followed by the methodology behind the LBM, as well as the computational setup for the jet-flat plate configuration. In Section III, the validation of the numerical model is described. In Section IV, the far-field aeroacoustic results are presented, including the sensitivity analysis of the jet-installation noise on geometric and flow parameters. The main characteristics of the phenomena involved in the scattering of the instability waves are described in Section V. Lastly, the concluding remarks are presented in Section VII.

II. Numerical Setup

A. Installed Jet Configurations and Flow Conditions

The installed jet model in this work replicates the NASA Glenn benchmark experiments [15, 16], where a flat plate is placed close to a single-stream jet nozzle (SMC000). The SMC000 is a round, convergent nozzle with an exit diameter D_j = 50.8 mm, used for studies on subsonic jets [15]. The primary convergent nozzle assembly has a 152 mm diameter inlet, followed by a contraction with a 5° taper angle up to the exit plane. Three geometric cases are investigated, where the length and radial position of the plate are varied, as shown in Fig. 1. For all selected cases, the surface is placed outside of the plume in order to avoid direct grazing from the jet. These cases were then chosen based on a jet spreading angle of 7° [15]. The plate is modeled with a 12.7 mm thickness and a chamfer angle of 40° at the trailing-edge. It also extends $0.75D_j$ upstream of the nozzle exit plane, to avoid scattering effects at the leading-edge. In the spanwise direction, the flat plate has a width of $36D_j$ to avoid scattering on the side edges as well.
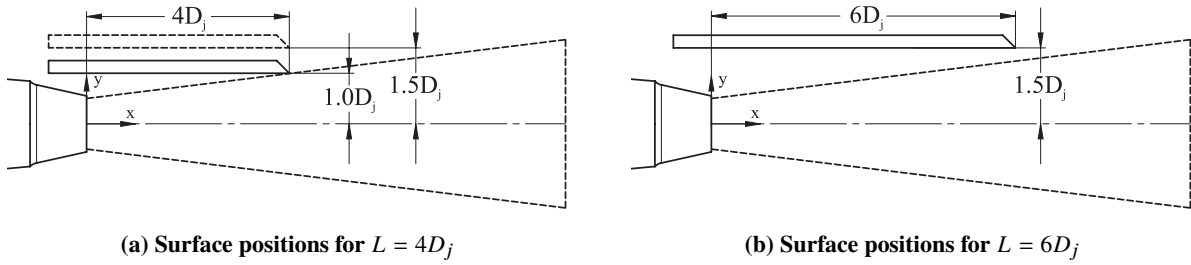
(a) Surface positions for $L = 4D_j$ **(b) Surface positions for** $L = 6D_j$

Fig. 1   Surface positions relative to the jet

The flow conditions for the numerical analyses are based on the setpoints 03, 07 and 46 from the NASA wind tunnel experiments [15]. Setpoint 03 is characterized by a cold, subsonic jet, with an acoustic Mach number $M_a = 0.5$ ($M_a = U_j/c_\infty$) and temperature ratio $T_R = 0.95$. Setpoints 07 and 46 represent cold and hot, high-subsonic jets ($M_a = 0.9$), respectively. The characteristics of each setpoint are included in Table 1, also in terms of nozzle pressure ratio (NPR). The Reynolds number is based on the nozzle exit diameter. Static flow parameters, such as ambient pressure and temperature, are obtained from the work of Brown [15]. The main results of this work are presented for setpoint 03, which is more compatible with a take-off condition. Thus, the other setpoints shall address the effect of Mach number and jet temperature on the installation noise, as shown in Section IV.C.

Table 1   Jet flow conditions for each setpoint

Setpoint	NPR [-]	T_R [-]	M_a [-]	Re [10^6]
03	1.197	0.950	0.50	0.592
07	1.860	0.835	0.90	1.068
46	1.227	2.700	0.90	1.066

B. Lattice-Boltzmann Method

The LBM consists in the computation of the discrete form of the Boltzmann equation by explicitly tracking the development of particle distribution functions at the microscopic scale. The Navier-Stokes equations can be recovered through the Chapman-Enskog expansion, and fluid properties such as density, momentum and internal energy are obtained through a local integration of the particle distribution [17]. The solution of the Boltzmann equation is performed on a Cartesian mesh (lattice), with an explicit time integration and collision model.

The low dissipation and dispersion of the LBM, coupled with a compressible and time-dependent solution, allow the sound field to be extracted directly from the pressure field [18]. However, this would require a fairly large computational domain with respect to the nozzle and plate dimensions, and a high degree of mesh refinement, even at regions far from the jet/surface, so that the number of points per wavelength would be sufficient for high-frequency far-field analyses. Therefore, to avoid high computational costs, the far-field noise can be computed via the Ffowcs-Williams and Hawkings equation [19], using the formulation 1A from Farassat, extended to a convective wave equation [18, 20]. The formulation is implemented in the time domain using a source-time dominant algorithm [21].

For that purpose, a permeable surface of arbitrary shape is defined encompassing the geometries of interest, such as the jet and the flat plate. The information on the fluctuations of flow properties is stored in this surface, where the integration is performed for the far-field noise propagation. This methodology allows for the inclusion of all noise sources placed inside the surface, such as the dipoles on the plate and the quadrupoles in the jet [22]. The characteristics of the FWH surface are included in Section II.C. The pressure integration is also performed on the flat plate solid surface, wherein only the dipole terms are taken into account, similarly to Curle's formulation [6].

The methodology described above is implemented in the commercial software Simulia PowerFLOW, which was used for the computations in this work. A new LBM-based entropy solver was recently introduced in PowerFLOW, with the second distribution function based on a specific scalar quantity [14]. This improved numerical errors that

occurred in previous versions of the software, that employed a Finite Difference Method solver for the entropy equation. Moreover, this new entropy solver, coupled with recent enhancements on the stability of flows at high Mach numbers, allows for more reliable computations of cold and hot jet flows [14].

Simulia PowerFLOW has been already used and validated for aero-engine aeroacoustic applications, in particular for fan broadband noise prediction in subsonic [23, 24] and transonic conditions [25]. A validation study for the isolated SMC000 jet flow has been also accomplished [14]. For an installed jet, computations were performed by Silva et al. [22]. The results, in terms of far-field noise spectra, showed a good agreement with experimental data, indicating the capability of the methodology to accurately predict the jet-installation noise.

C. Computational Setup

The tridimensional computational setup is comprised by two main geometrical features: the SMC000 nozzle and the flat plate. The physical nozzle is completely modelled in the domain. An inlet boundary condition is placed $8D_j$ upstream of the nozzle exit plane to avoid interferences with the actual jet flow. The inlet characteristics are defined based on the jet total pressure (obtained from each setpoint), whereas the outlet of the computational volume is defined as the reference pressure (atmospheric). A zig-zag trip was included inside of the nozzle to force a fully turbulent boundary layer. It has a thickness of 1 mm ($0.02D_j$) and wavelength of 1.62 mm ($0.03D_j$), and it is positioned $1.5D_j$ upstream of the exit plane. This setup has been already validated for isolated jet simulations by van der Velden et al. [14]. Therefore, the same strategy is adopted in this work, for the installed case. The main components of the setup are shown in Fig. 2.
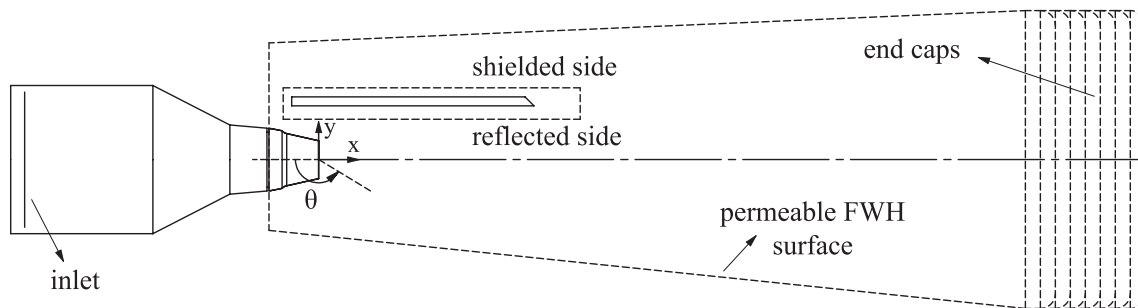

Fig. 2   Components of the computational setup

A permeable Ffowcs Williams-Hawkings (FWH) surface is included in the model, as shown by the dashed lines in Fig. 2. The information on unsteady flow properties is stored on this surface, for the far-field noise calculation. The shape and dimensions of the FWH surface were chosen so that the same geometry could be used for all installed cases, as well as the isolated jet for consistency. In order to reduce the size of the stored data, the permeable surface does not encompass the entire flat plate span. By considering the 7° spreading angle of the jet, the plume has a cross-section diameter of $2.5D_j$ at the trailing-edge position for the longest plate case. Therefore, the FWH is designed with a width of $10D_j$, which is likely to contain the region where the jet-plate interaction is strongest. In the streamwise direction, it extends up to $22D_j$, relative to the nozzle exit plane. Thus, it is capable of capturing the quadrupoles from the jet, as well as the dipoles distributed on the surface.

Hydrodynamic perturbations occurring near the boundaries of the FWH must be avoided, since they contaminate the results with spurious source of sound. Thus, the side faces of the permeable surface are positioned far from the jet shear layer. A cutout is included at the nozzle and flat plate regions, from where the data is removed during the computations. In the axial direction, making the permeable surface long enough to avoid contact with the jet would result in high computational costs. Therefore, 7 outflow surfaces (or end-caps) are placed at the end of the FWH. The far-field pressure obtained from each cap (located at different streamwise positions) is phase-averaged, so that the uncorrelated noise produced by the eddies crossing the FWH can be removed from the final far-field spectra [26].

A free-stream condition is added to the simulation domain, with a velocity of 1% of the jet nominal speed. This is done to ensure the dissipation of eddies that escape the jet shear layer. This free-stream speed can be considered negligible when compared to the jet velocity. Therefore, this condition will not alter the flow-field characteristics of the shear layer or the far-field noise results. Acoustic sponges, which consist in regions of increased viscosity, are also

added around the entire geometry and inside of the nozzle to prevent wave reflection at solid boundaries and at the walls of the computational domain [27]. The progressive coarsening of the grid towards the far-field boundaries also contributes to the damping of acoustic waves, reducing the effects from reflection.

The computational domain is divided into regions with different mesh refinements (Variable Resolution - VR), with a change in element size by a factor of 2, for adjacent regions. A global mesh resolution is then defined, based on the number of elements in a characteristic length (nozzle exit diameter). Thus, different levels of mesh refinement, corresponding to coarse, medium and fine can be generated. The characteristics of each grid are included in Section III. The element size is kept constant on the jet plume up to $10D_j$ downstream of the nozzle exit plane, as well as between the flat plate and the plume. A further level of refinement is added downstream of the nozzle lip to properly capture the formation of the shear layer and the hydrodynamic fluctuations.

Similarly as performed in the NASA benchmark experiments [15], the far-field noise levels are computed at a microphone arc array, centered at the nozzle exit plane. The radius of the array is defined as $100D_j$. Microphones are placed at an interval of 5°, ranging from $\theta = 50°$ to $\theta = 165°$ ($\theta = 180°$ corresponding to the jet axis). The computations are also performed on both shielded and reflected sides of the plate. An azimuthal array is also defined around the nozzle exit plane, with 12 microphones spaced of 30°.

III. Grid Convergence and Validation

A mesh convergence study is required to assess the sensitivity of the numerical results to the discretization of the computational domain. In this work, three different grid sizes are investigated: coarse (resolution = 32), medium (resolution = 45), and fine (resolution = 64). The resolution of a grid is based on the number of elements in the nozzle exit diameter. The selected case corresponds to an installed jet with a flat plate length $L = 4D_j$ and distance to the jet axis $h = 1D_j$, where the surface is positioned closest to the plume. The characteristics of each grid are shown in Table 2. The results are also compared with the experimental data from NASA Glenn [15, 28], for validation purposes. The grid convergence and validation are evaluated in terms of the aerodynamic properties of the jet (velocity profiles) and far-field noise spectra.

Table 2   Grid characteristics for convergence analysis

Grid	Resolution	Voxel Size at Nozzle Exit [mm]	Number of Voxels [10^6]	kCPUh
Coarse	32	1.588	153.2	5.5
Medium	45	1.129	371.2	23
Fine	64	0.794	942.4	48

A. Flow Field

The aerodynamic measurements from the NASA Glenn installed jet studies are included in the work of Brown and Wernet [29]. In the experiments, the jet flow field was measured with Particle Image Velocimetry (PIV) at streamwise and cross-stream planes. For setpoint 03 ($M_a = 0.5$), which is the focus of this work, the experimental data are available only for the isolated configuration, which were also obtained from PIV measurements [28]. For all the cases investigated in this work, the flat plated is situated in the linear hydrodynamic field of the jet, and no grazing occurs on the surface. Therefore, no significant changes are expected to occur in the flow at the jet centerline (y = 0 mm) and lipline (y = 25.4 mm) due to the presence of the plate. Flow-field snapshots of the installed jet, for both surface lengths, are shown in Fig. 3, at the radial positions closest to the jet.

From the snapshots shown in Fig. 3, the jet is shown to be fully turbulent, indicating that the trip forces boundary layer transition inside the nozzle. There is also no grazing of the jet on the surface, for both geometries, and no visible indication that the jet flow-field is altered by the presence of the flat plate. Thus, the aerodynamic results of the numerical setup can be validated through flow-field comparisons based on the isolated jet case. The mean (time-averaged) and fluctuating velocity profiles, normalized by the jet nominal speed (U_j), are shown in Fig. 4, for the jet centerline, and in Fig. 5, for the jet lipline. The curves are plotted for all three grid resolutions, as well as the experimental results from NASA. The results for the installed jet ($L = 4D_j$ and $h = 1D_j$) are also included, to verify that there are no changes on the velocity profiles due to the presence of the nearby surface.
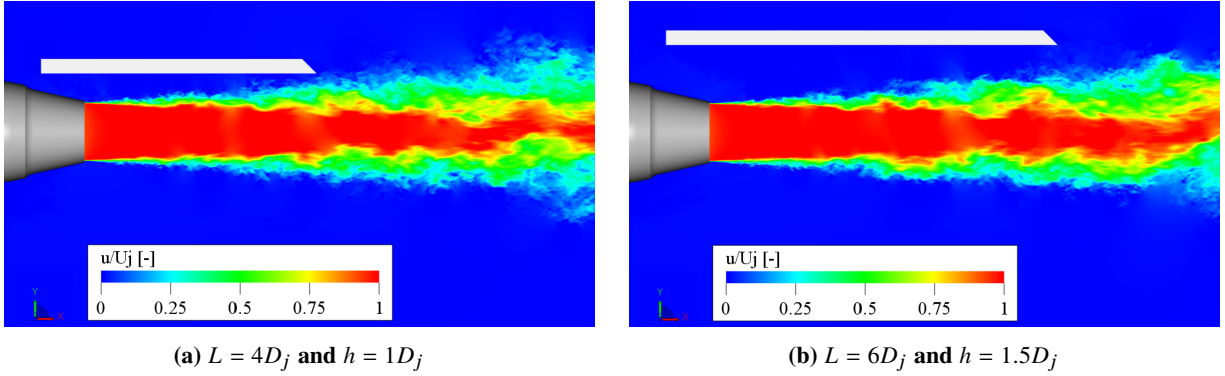
(a) $L = 4D_j$ **and** $h = 1D_j$

(b) $L = 6D_j$ **and** $h = 1.5D_j$

Fig. 3   Snapshots of the installed jet velocity field
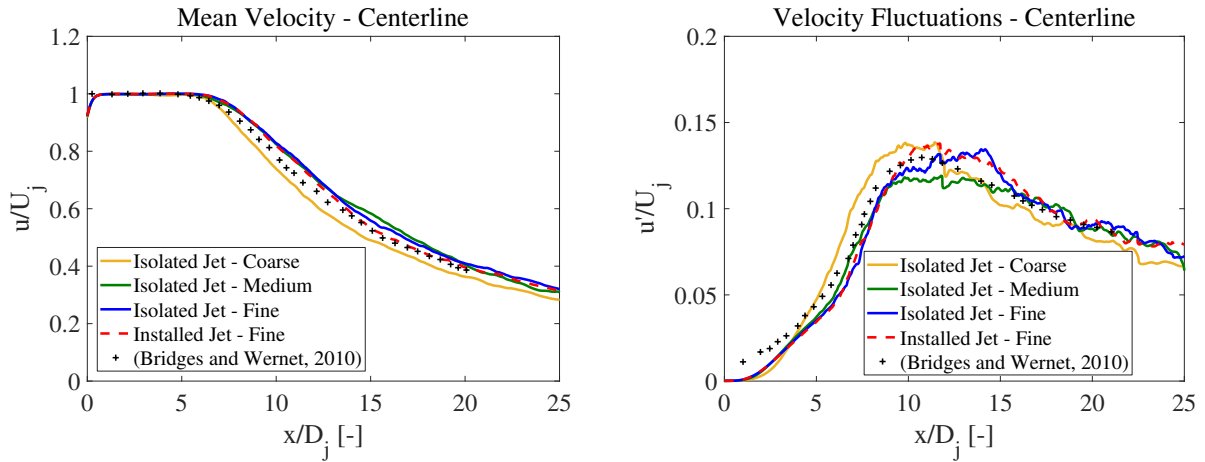

Fig. 4   Axial mean velocity and fluctuation profiles at the nozzle centerline, for different grid resolutions
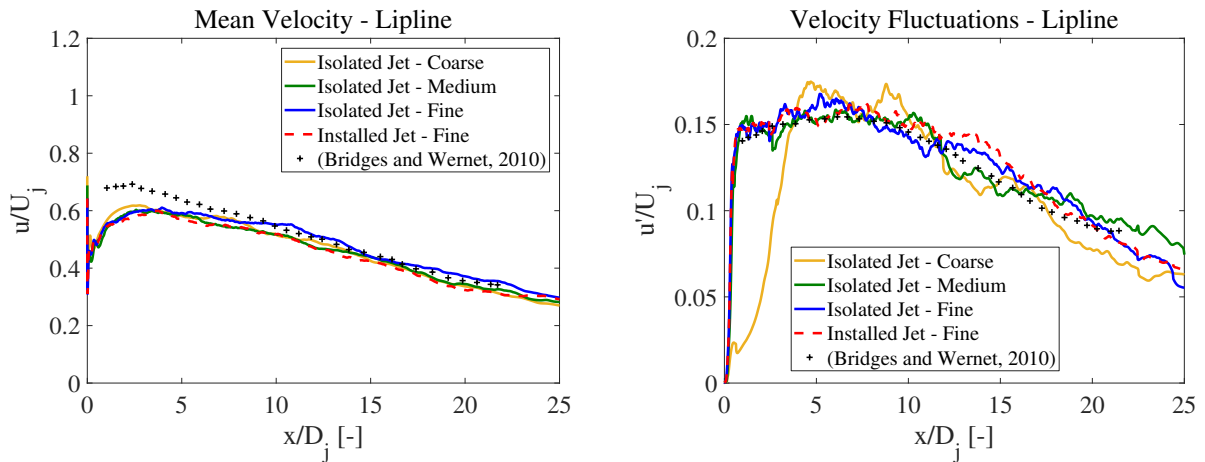

Fig. 5   Axial mean velocity and fluctuation profiles at the nozzle lipline, for different grid resolutions

At the centerline, the potential core region is well captured by the simulations, extending up to approximately 6.5 nozzle diameters from the exit plane. There is a slight overprediction of the centerline velocity decay, when compared to the experimental results. However, the variations are small, on the order of 4% of the jet nominal velocity. The velocity fluctuations are well captured, especially after the end of the potential core. At the lipline, the results for the

mean velocity match well from $x/D_j = 5$ and downstream. In their publication, Bridges and Wernet [28] state that the experimental results near the nozzle lip have a high level of uncertainty, due to the proximity between the measurement probe and the surface. The fluctuations at the lipline also show a good agreement with the experimental data, except for the coarse mesh. For all the profiles shown above, the installed and isolated cases have nearly identical results, indicating that there is no effect on the jet properties caused by the presence of the flat plate. Therefore, the flow-field results for the numerical setup are considered to be validated.

B. Far-field Acoustic Spectra

The far-field spectra from the simulations of the installed configuration are compared to the experimental results of Brown [15]. The results are displayed for the reflected side of the plate, at two polar angles: one at the sideline direction ($\theta = 90°$) and the other closer to the jet axis ($\theta = 160°$). The one-third octave sound pressure level (SPL) spectra, as a function of Strouhal number ($St = f \times D_j/U_j$), are shown in Fig. 6, for a surface with $L = 4D_j$ and $h = 1D_j$.
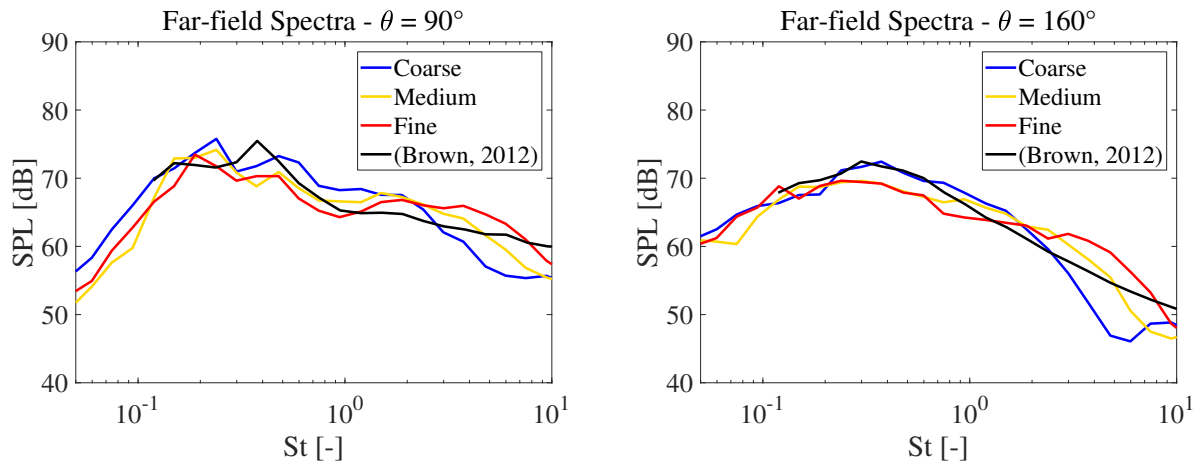

Fig. 6   Grid convergence and validation of aeroacoustic results for the installed jet ($L = 4D_j$ **and** $h = 1D_j$)

From the curves of Fig. 6, the spectral shape of the installed jet is correctly predicted by the simulations. On both polar angles, a similar trend occurs, as the mesh resolution is increased. At low frequencies, the noise levels tend to decrease from the coarse to the medium case, and then it stabilizes, as shown by the fine curve. For medium and high frequencies, the effect of grid resolution is more evident. There is a region of higher noise levels, compared to the experimental results, up to the cut-off frequency. At this point, the slope of the spectra changes, and a significant decrease in noise levels follows. This occurs due to the inability of smallest element size of the mesh to capture fluctuations at those frequencies. For the coarse mesh, the cut-off frequency occurs at $St \approx 1.8$, whereas for the fine case, it occurs at $St \approx 4$. The maximum deviation between the results for the fine mesh and the experiments are approximately 3 dB, which shows the capability of the model to correctly predict the jet-installation noise. The results shown in the next sections of this manuscript are then obtained for the fine resolution grid.

IV. Far-field Analyses

A. Spectral Analysis and Directivity

In this section, the far-field noise spectra of the installed jet are analyzed and compared with the isolated case. The third-octave spectra are shown in Fig. 7, for a surface with $L = 4D_j$ and $h = 1D_j$, at the sideline direction and closer to the jet axis, and for observer positions on both reflected ($\theta = 90°$ and $\theta = 160°$) and shielded ($\theta = 270°$ and $\theta = 200°$) sides of the plate.

In the sideline direction, the installed jet displays higher noise levels than the isolated case, particularly at low frequencies, up to $St = 0.7$. The largest amplification occurs at $St = 0.19$, with installation penalties of approximately 14.7 dB. In this amplification region, the spectra at the reflected and shielded sides display similar levels, which is consistent with the results from Head and Fisher [9]. This indicates that the dominant source is located at the
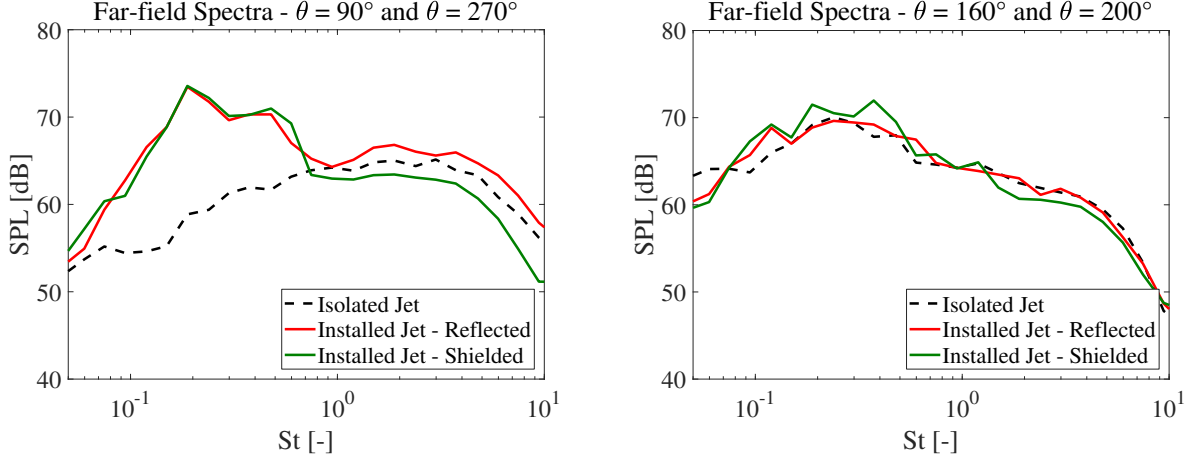
Fig. 7 **Far-field spectra of the installed jet, at the reflected and shielded sides of the plate ($L = 4D_j$ and $h = 1D_j$), compared to the isolated configuration**

trailing-edge of the plate so that there is no effect of sound reflection or shielding. Therefore, the dominant noise generation mechanism for this frequency range is the scattering of the near-field hydrodynamic waves at the trailing-edge of the surface. For $St > 0.7$, the spectra of the installed cases are dominated by the quadrupole jet noise either reflected or shielded by the plate. At the reflected side, the noise levels are approximately 3 dB higher than the isolated case, which is consistent with reflection on a half-plane [11].

By moving towards the jet axis, the installation effects are no longer visible and the spectra become similar to that of the isolated jet. This occurs due to the directivity properties of the dominant source in the installed configuration. Ffowcs-Williams and Hall [7] demonstrated that the scattering by a half-plane has a characteristic cardioid-shaped sound directivity. The maximum amplitude is obtained in the upstream jet axis direction ($\theta = 0°$), whereas downstream ($\theta = 180°$) there is no propagation. Therefore, the scattering effects are not expected to be visible towards the jet axis. Moreover, the isolated jet displays higher noise levels in this region, compared to the sideline direction. This is due to the superdirective characteristic of the jet, with exponentially increasing noise towards the axis [8]. Directivity plots are shown in Fig. 8, in terms of Overall Sound Pressure Level (OASPL), integrated up to $St = 4$ (cut-off frequency), which illustrate this behavior.
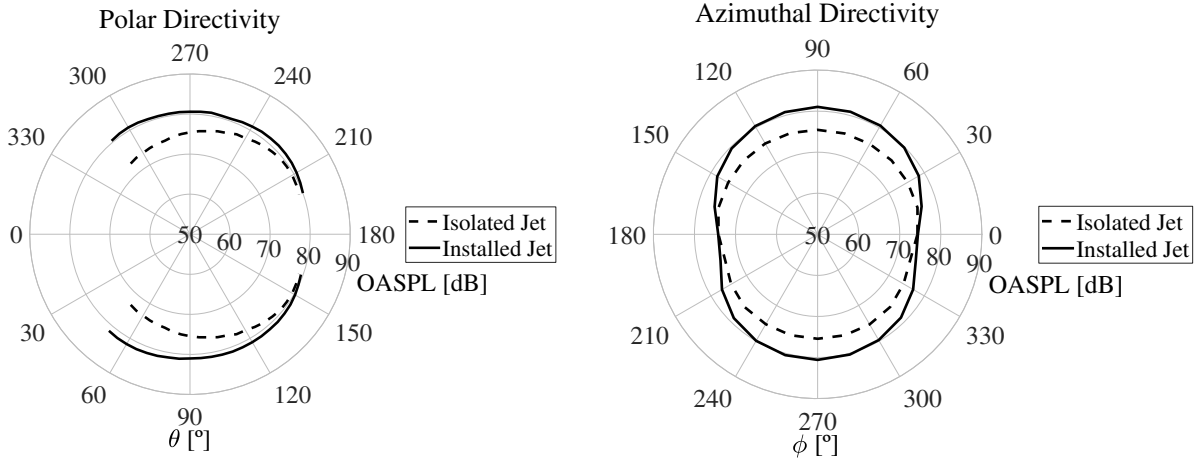

Fig. 8 **Polar and azimuthal directivities of the isolated and installed jets ($L = 4D_j$ and $h = 1D_j$)**

In the polar direction, the maximum installed noise levels are shown to occur at $\theta \approx 50°$. Smaller angles could not be computed due to the presence of the nozzle, which acts as a shielding body. However, the trend of the curves is consistent with the cardioid directivity. The isolated levels are also found to be lower in the upstream direction, and

8

therefore, the penalties are largest in that region. Approaching the jet axis, the curves for isolated and installed cases display the same amplitudes, indicating that the quadrupole sources have become dominant. In the azimuthal direction, the OASPL values were obtained for a fixed polar angle of $\theta = 90°$. The isolated jet displays an axisymmetric behavior, with similar noise levels at all azimuthal angles. For the installed jet, larger noise levels on the order of 5 dB are obtained in the directions normal to the flat plate ($\phi = 90°$ and $\phi = 270°$). In the spanwise direction of the plate, the levels are shown to be the same as the isolated case. This is consistent with the presence of dipoles, with axes perpendicular to the surface. These results are in agreement with the ones from Head and Fisher [9].

B. Effect of Surface Geometry

In this section, the influence of geometrical properties of the flat plate on the overall installed jet noise is assessed. The effects of surface length and radial position of the plate, relative to the jet, are shown in Figs. 9a and 9b, respectively. The far-field spectra were obtained at a polar angle $\theta = 270°$ (shielded side of the plate), which allows for a better visualization of the frequency range where the installation effects occur. This range is thus defined based on the points where the spectra for the installed cases cross the isolated curve.
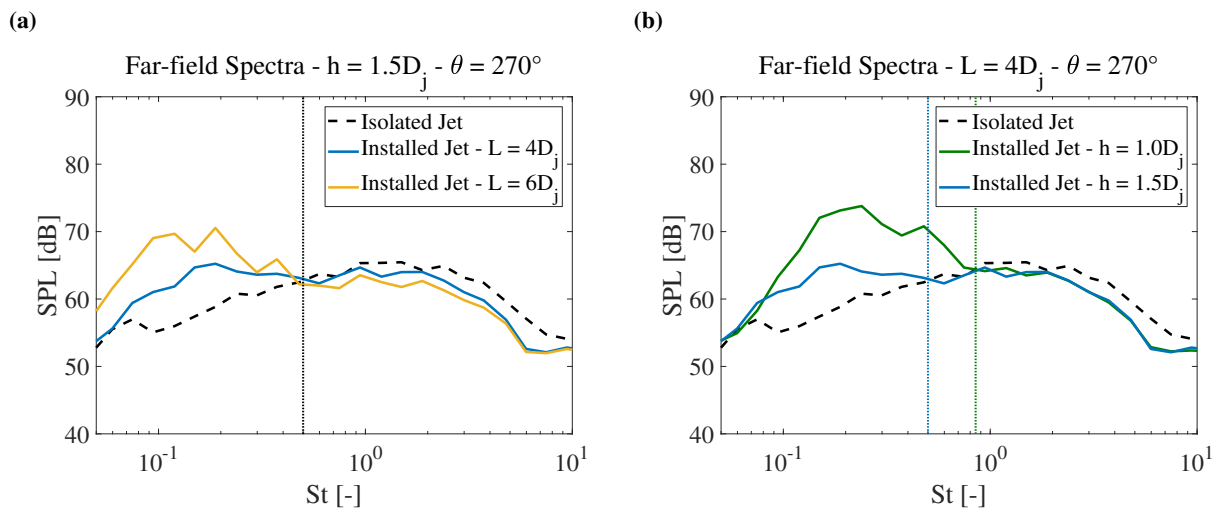
(a)

(b)

Fig. 9   Far-field spectra for different geometric configurations of the installed jet (change in surface length and radial position)

The spectra shown in Fig. 9a were obtained for surfaces with lengths $L = 4D_j$ and $L = 6D_j$, at a radial position $h = 1.5D_j$. It can be seen that the sound pressure levels are higher for the case with the longer plate, with differences of approximately 8 dB, for $St = 0.12$. This occurs due to the increase in the energy content of large-scale structures, when moving in the downstream direction of the jet. Since these structures generate low-frequency hydrodynamic pressure waves, the scattering effects will also be amplified for the case with the longer surface. Despite this difference at low frequencies, the upper frequency limit where the installation effects occur is the same for both plates, as shown by the dotted line. It was shown by Arndt et al. [30] that the high wavenumber (small-scale) structures show similar characteristics and amplitude throughout the flow, in the streamwise direction, as opposed to the larger scales. Therefore, at these higher frequencies, the scattering will not likely be affected by changes in the surface length (streamwise changes).

The effect of changing the radial distance of the plate, relative to the jet centerline, is shown in Fig. 9b, for surfaces positioned at $h = 1D_j$ and $h = 1.5D_j$, with a fixed length $L = 4D_j$. It can be seen that, by moving the surface closer to the plume, there is an amplification in the sound pressure levels, with a maximum of 9.8 dB, at $St = 0.24$. This amplification was found to be more pronounced at the mid- and upper limit of the frequency range where the installation effects occur. There was no visible effect on lower frequencies ($St < 0.1$). Moreover, the frequency range of the noise amplification also increases for the case with the surface closer to the jet. This is shown by the blue and green dotted lines, representing the crossing point on the spectra, for the cases with $h = 1.5D_j$ and $h = 1D_j$, respectively. This is likely to occur due to the increased proximity of the surface to smaller scale eddies that generate higher frequency noise when scattered.

C. Effect of Jet Velocity and Temperature

In this section, the effect of the jet velocity and temperature on the scattering by a nearby flat-plate is addressed. The former is performed by comparing setpoints 03 and 07, which consist of subsonic cold jets with acoustic Mach numbers $M_a = 0.5$ and $M_a = 0.9$, respectively. The latter is carried out by comparing setpoints 07 and 46, with the same acoustic Mach number, but with different temperature ratios. Setpoint 46 consists in a high-subsonic hot jet with $T_R = 2.7$. The far-field spectra of the installed jet for different setpoints are shown in Fig. 10, represented by the solid curves. The noise levels for the isolated configuration at each condition are also plotted for reference, represented by the dashed lines.
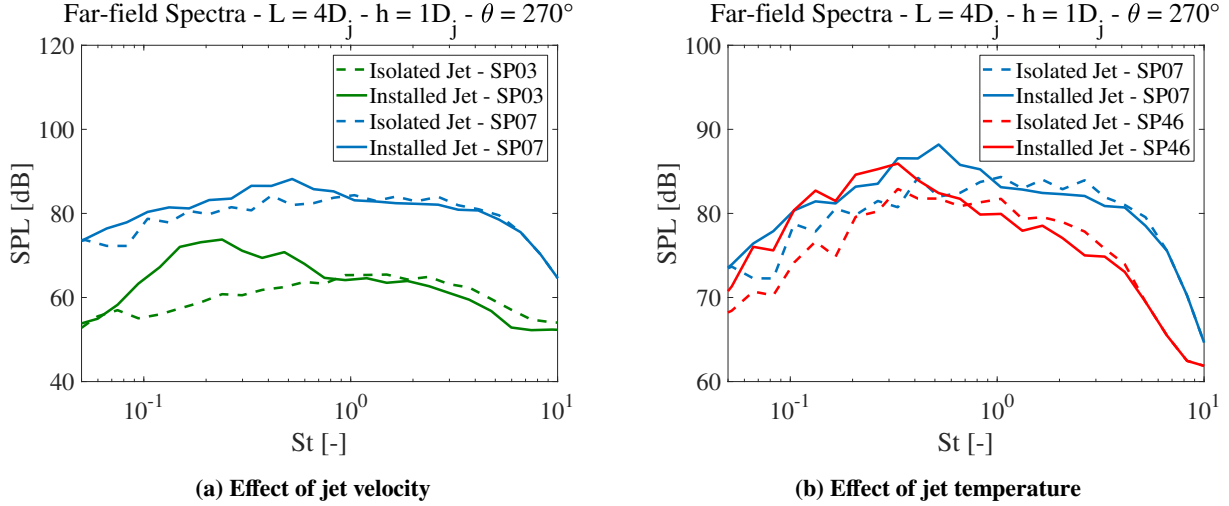

(a) Effect of jet velocity

(b) Effect of jet temperature

Fig. 10   Effect of jet flow conditions on the installation noise

From Fig. 10a, it can be seen that the curves for the isolated jet at setpoints 03 and 07 have approximately the same spectral shape, with a nearly constant amplitude difference for every frequency value. This is due to the scaling of the far-field noise of an isolated jet, dominated by quadrupole terms, with the eight power of the velocity (U_j^8) in the sideline direction [31]. The installed configuration, on the other hand, shows different trends for each jet flow condition. For setpoint 07, the installation effects account for a maximum amplification of 6 dB, compared to approximately 15 dB in setpoint 03. It was shown by Ffowcs-Williams and Hall [7] that the noise generated due to trailing-edge scattering has a dependence on (U_j^5). Therefore, when increasing the Mach number of the jet, the quadrupole terms tend become comparable to the dipoles, even at polar angles away from the jet axis. The frequency range of the installation effects, in terms of Strouhal number, does not seem to be largely affected by the increase in speed.

The effect of the jet temperature, as shown in Fig. 10b was verified for a high Mach number jet. At low frequencies, up to $St = 0.3$, there are no apparent changes on the spectral shape or amplitude when the temperature of the jet is increased. However, for the installed case at $St > 0.3$, the noise levels for the heated jet tend to sharply decrease in comparison to the unheated case. This phenomenon is also visible for the isolated jet, but at a lower magnitude. The same trend was verified in the work of Brown [15], and it was attributed to a shortening of the potential core of the jet due to the increased temperature, with a consequent reduction of the jet spreading angle. This results in a rearrangement of the eddies inside of the plume, which will have different characteristics to those of the unheated jet. Since the scattering of pressure waves is dependent on the local characteristics of the eddies, the installation noise is also affected by changes in temperature.

The scaling of the noise levels with the jet speed is plotted in Fig. 11 for the isolated and installed jets, based on the results of setpoints 03 and 07. The pressure fluctuations on the surface are also integrated and propagated to the far-field so that only the contribution of the acoustic dipoles are taken into account. The noise levels for the isolated jet are given by the black solid curve, and they are seen to agree well with the U_j^8 law for turbulent mixing noise in the sideline direction [31]. The overall installed jet, given by the red curve, approximates more the U_j^6 curve, whereas the integration of the surface pressure fluctuations (blue curve) has a trend closer to U_j^5, which is consistent with the predictions of Ffowcs-Williams and Hall for trailing-edge scattering [7]. The behavior of the overall installed jet is likely related to the increased significance of the quadrupole terms for higher velocities, changing the overall slope of the curve.
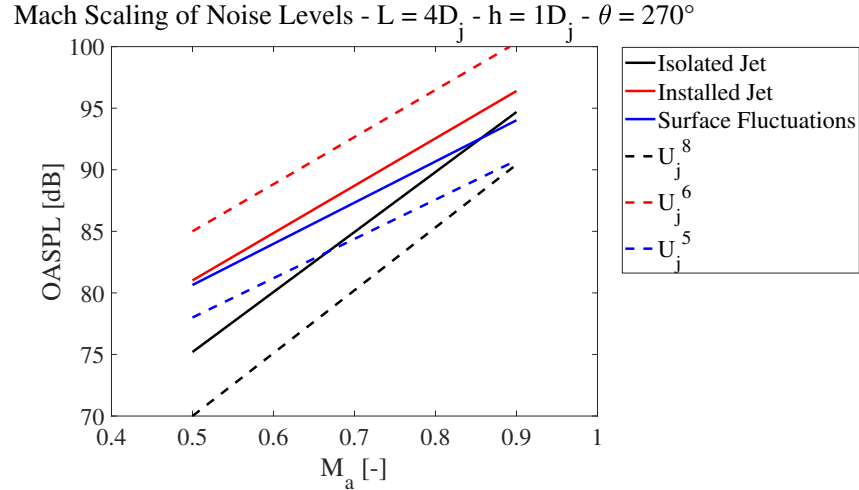
Fig. 11   Scaling of far-field noise of the isolated and installed jets, as well as the surface pressure fluctuations, with the acoustic Mach number

V. Installation Effects and Trailing-Edge Scattering

A. Time Derivative of the Pressure Field

The time derivative of the near pressure field is calculated to allow the visualization of the different waves radiated from the jet flow. Fast-changing fluctuations are emphasized, which allows for the evanescent field of the jet to be easily observed. Moreover, since the installation effects occur at a specific frequency range, it is interesting to apply a band-pass filter on the data, to generate plots for specific frequency bands. Snapshots of the dilatation field, for the isolated and installed jets, are shown in Figs. 12 and 13, respectively, for a frequency band of $0.18 < St < 0.21$, which is consistent with the far-field spectral peak. The high saturation of the contours is necessary to visualize the propagation of the pressure waves outside of the plume.
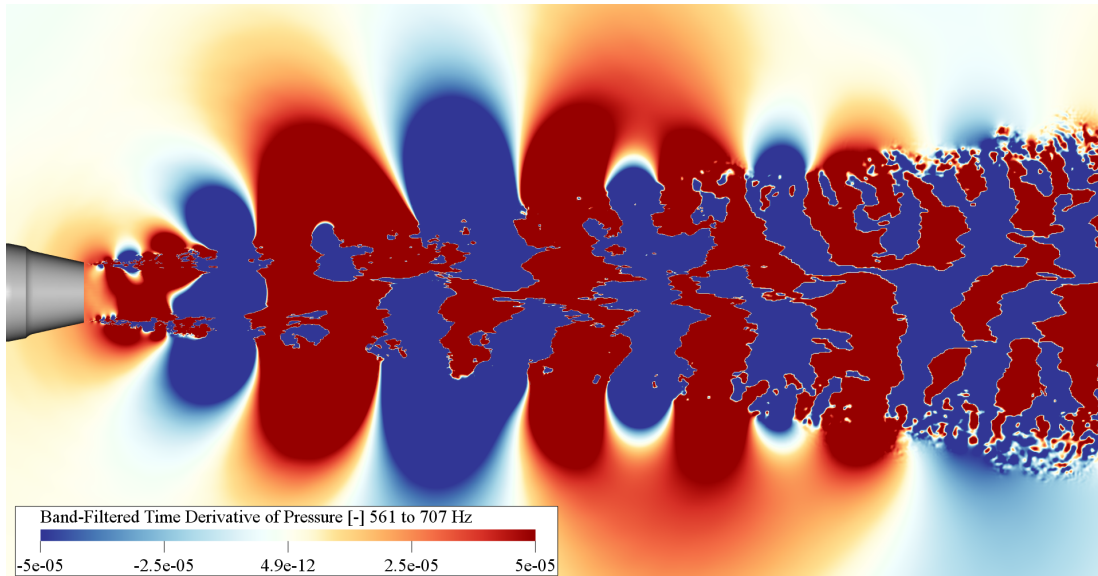

Fig. 12   Band-pass filter of the dilatation field on the isolated jet $(0.18 < St < 0.21)$

The snapshot of the dilatation field of the isolated jet shows pressure waves convecting with the jet. Given the low Mach number of the jet in setpoint 03 ($M_a = 0.5$), it is expected that a large portion of those waves will be convected

at subsonic speeds. A distinct change in amplitude, characterized by growth, saturation and decay can be observed. Therefore, due to this spatial modulation, a small portion of the energy from the waves in the evanescent near-pressure field is acoustically matched, resulting in noise propagation to the far-field [32].
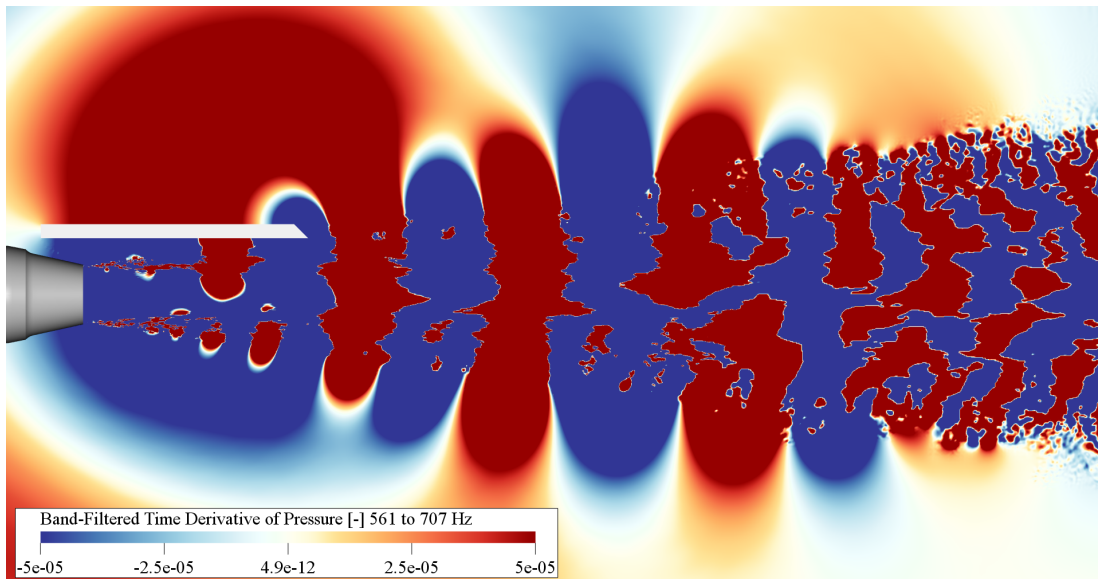

Fig. 13   Band-pass filter of the dilatation field on the installed jet ($0.18 < St < 0.21$)

For the installed jet, strong pressure regions are generated at the trailing-edge of the surface. The pressure perturbations from the jet impinge on the surface, and, as they reach the geometric discontinuity, these waves undergo a change of impedance, when moving from a bounded to an unbounded region. This phenomenon leads to their scattering and consequent propagation to the far-field so that the Kutta condition can be satisfied. The scattered waves tend to propagate perpendicularly to the surface, as well as in the upstream direction, characteristic of the cardioid directivity. In the downstream direction, the pattern is similar to the isolated case, which is consistent with the far-field results. The scattered waves on the reflected and shielded sides of the plate have opposing signs, indicating the phase-shift of π, as was described by Head and Fisher [9]. This pattern of out-of-phase waves travelling upstream with the same speed indicates that a region of zero-pressure occurs at the leading-edge of the plate, where the Kutta condition is again satisfied.

B. Surface Pressure Fluctuations
The pressure fluctuations on the surface can be extracted and displayed as a function of the axial position. This allows for an analysis on the strength of the local acoustic dipoles, and where they are mostly concentrated. Therefore, the plate is divided into several spanwise strips, where the fluctuations are integrated. Afterwards, a Fourier transform is applied to the integrated signals so that the analysis can be conducted in the frequency domain. The contour plots in Fig. 14 show the spectra at several axial positions on the flat plate, for the case with $L = 4D_j$ and $h = 1D_j$, on the lower and upper surfaces, respectively.

On the bottom side of the plate, the maximum fluctuations occur at $x/L = 0.9$ and $St = 0.2$. This is consistent with one of the peaks on the far-field spectrum. The other far-field peak ($St = 0.43$) also displays significant levels on the surface spectra, at the same axial position. Given the high amplitude of the fluctuations at that location, it is likely that there is a strong impingement of hydrodynamic pressure waves, before the scattering occurs at the trailing-edge. Towards the leading-edge of the plate, small fluctuations are seen at different frequency values. These are likely related to the impingement of the scattered acoustic waves, which travel upstream. A similar behavior is obtained on the upper side, where there is no incident field from the jet, but only the scattered acoustic field. The axial position of maximum fluctuations on the lower side does not necessarily occur at the trailing-edge, but slightly upstream. This is likely due to destructive interference, happening near that region. As shown in the dilatation field plots, a phase shift exists between two waves that are sequentially scattered. Therefore, this phase difference between incident and scattered fields shall be highest at the trailing-edge and it will tend to move the position of maximum fluctuations upstream. On the upper
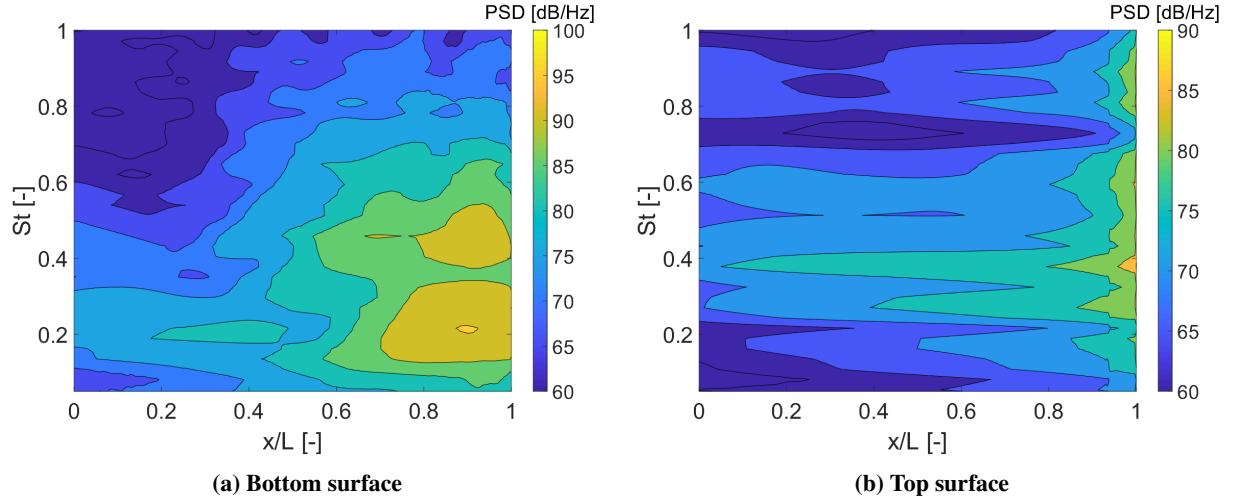
(a) Bottom surface   (b) Top surface

Fig. 14   Spectra of pressure fluctuations on the surface at different axial positions (L = $4D_j$ and h = $1D_j$)

side, since there is only the scattered field, no interference occurs and the maximum fluctuations are obtained at the trailing-edge.

    The pressure fluctuations on the plate can also be integrated and propagated to the far-field through the FWH solid formulation [19]. This is equivalent to apply the surface integral term of Curle's formulation [6], which neglects the contribution of the turbulent mixing in the far-field noise calculation. Thus, only the contribution of the acoustic dipoles on the plate is considered. The integration is performed for a spanwise length of $10D_j$ in order to match the dimensions of the permeable FWH surface. The far-field spectrum of the fluctuations is shown in Fig. 15a, in terms of Power Spectral Density (PSD) for a better visualization, for an observer position of $100D_j$ and $\theta = 90°$, along with the isolated and installed jet spectra obtained from the permeable surface integration.
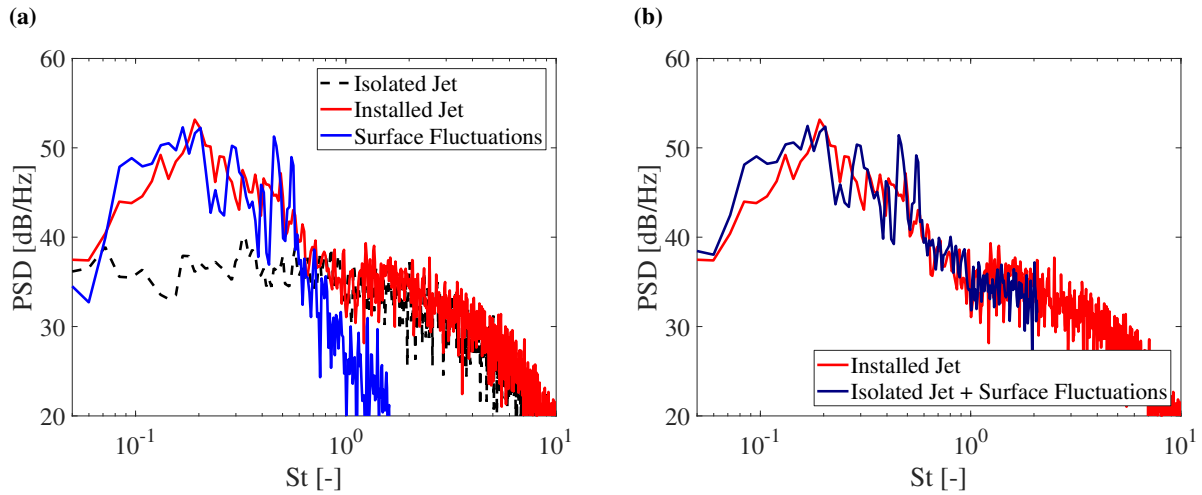

Fig. 15   Far-field spectra of the pressure fluctuations on the flat plate, compared to results the from the permeable FWH surface (isolated and installed jets)

    It can be seen from Fig. 15a that the spectra from the pressure fluctuations on the surface aligns with the curve of the overall installed jet, for the entire frequency range where the installation effects occur. This indicates that the scattering of hydrodynamic waves by the flat plate is indeed the dominant noise generation mechanism for the installed jet. Moreover, by considering the jet and the plate as uncorrelated sources, their noise levels can be summed, as shown in Fig. 15b. The sum of the far-field noise produced by the separate sources provides the same levels as the overall installed jet, indicating that there is no significant change on the quadrupole sources due to the presence of the plate.

13

VI. Conclusions

A high-fidelity numerical investigation of an installed jet was performed using the Lattice-Boltzmann Method. A simplified configuration, comprised by a single-stream nozzle and a nearby flat plate was chosen for the analyses. The simulation results were validated through comparison with experimental data, obtained from tests at NASA Glenn. The far-field spectral results, obtained from the Ffowcs-Williams Hawkings analogy, indicated a large noise increase at low and mid frequencies, followed by reflection or shielding of the quadrupole jet noise. Through dilatation field plots, this amplification was shown to be caused by the hydrodynamic waves from the jet that are bounded by the plate and, as they reach a geometric discontinuity (surface trailing-edge), they are scattered to the far-field as noise. This new source displayed a dipolar characteristic in the azimuthal direction, and a cardioid directivity pattern in the polar direction. Maximum noise levels were obtained in the upstream direction of the jet axis, whereas in the downstream direction there was no amplification.

Through integrations of the pressure fluctuations on the surface, it was found that the acoustic dipoles are the dominant noise sources at low frequencies, for the installed case. There was no visible change in the quadrupole terms due to the presence of the flat plate, so that they can be considered uncorrelated to the dipole sources. The geometry of the plate was also found to affect the far-field noise. By increasing the length, the trailing-edge is placed in a region dominated by larger-scale structures, which tend to generate low-frequency noise. However, the upper frequency limit of the installation effects remains unchanged. On the other hand, by moving the plate closer to the jet in the radial direction, there is an increase in sound especially at higher frequencies. This is likely due to the effect of compactness of the sources, relative to the trailing-edge. It is expected that only non-compact eddies, at a certain distance from the trailing-edge, are amplified through the scattering, whereas the compact eddies display the same characteristics as free turbulence. This shall be addressed in further works.

The characteristics of the jet flow, such as the velocity and temperature were shown to affect differently the installation effects. For high Mach number jets, the noise amplification caused by the trailing-edge scattering is comparable to the component of turbulent mixing. Therefore the installation effects are not as significant in this condition. For heated jets, a reduction in noise levels for the installed case was obtained at medium frequencies, which is likely related to changes in the structures of the jet, since the potential core is shortened and the spreading angle is decreased. The effect of temperature in the jet flow properties and, consequently, in the installation effects shall also be addressed in further works.

Acknowledgments

References

[1] Huff, D. L., "Noise Reduction Technologies for Turbofan Engines," *NASA/TM—2007-214495*, 2007, pp. 1–17.

[2] SenGupta, G., "Analysis of Jet-Airframe Interaction Noise," *AlAA 8th Aeroacoustics Conference*, Atlanta, Georgia, USA, 1983.

[3] Brown, W. H., and Ahuja, K. K., "Jet and Wing/Flap Interaction Noise," *AIAA/NASA 9th Aeroacoustics Conference*, WiIIiamsburg, Virginia, 1984. doi:10.2514/6.1984-2362.

[4] Mengle, V. G., Brusniak, L., Elkoby, R., and Thomas, R. H., "Reducing Propulsion Airframe Aeroacoustic Interactions with Uniquely Tailored Chevrons: 3. Jet-Flap Interaction," *12th AIAA/CEAS Aeroacoustics Conference*, Cambridge, MA, 2006. doi:10.2514/6.2006-2435.

[5] Belyaev, I., Faranosov, G., Ostrikov, N., and Paranin, G., "A parametric experimental study of jet-flap interaction noise for a realistic small-scale swept wing model," *21st AIAA/CEAS Aeroacoustics Conference*, Dallas, TX, 2015. doi:10.2514/6.2015-2690.

[6] Curle, N., "The influence of solid boundaries upon aerodynamic sound," *Proceedings of the Royal Society A 231*, 1955, pp. 505–514. doi:10.1098/rspa.1955.0191.

[7] Ffowcs-Williams, J. E., and Hall, L. H., "Aerodynamic sound generation by turbulent flow in the vicinity of a scattering half plane," *Journal of Fluid Mechanics*, Vol. 40, No. 4, 1970, pp. 657–670. doi:10.1017/S0022112070000368.

[8] Cavalieri, A. V., Jordan, P., Colonius, T., and Gervais, Y., "Axisymmetric superdirectivity in subsonic jets," *Journal of Fluid Mechanics*, 2012. doi:10.1017/jfm.2012.247.

[9] Head, R. W., and Fisher, M. J., "Jet/Surface Interaction Noise: - Analysis of Farfield Low Frequency Augmentations of Jet Noise due to the presence of a Solid Shield," *3rd AIAA Aero-Acoustics Conference*, Palo Alto, CA, USA, 1976. doi:10.2514/6.1976-502.

[10] Lawrence, J. L. T., Azarpeyvand, M., and Self, R. H., "Interaction between a Flat Plate and a Circular Subsonic Jet," *17th AIAA/CEAS Aeroacoustics Conference*, Portland, OR, USA, 2011. doi:10.2514/6.2011-2745.

[11] Cavalieri, A. V., Jordan, P., Wolf, W. R., and Gervais, Y., "Scattering of wavepackets by a flat plate in the vicinity of a turbulent jet," *Journal of Sound and Vibration*, Vol. 333, No. 24, 2014, pp. 6516–6531. doi:10.1016/j.jsv.2014.07.029.

[12] Lyu, B., Dowling, A. P., and Naqvi, I., "Prediction of installed jet noise," *Journal of Fluid Mechanics*, Vol. 811, 2017, pp. 234–268. doi:10.1017/jfm.2016.747.

[13] Piantanida, S., Jaunet, V., Huber, J., Wolf, W., Jordan, P., and Cavalieri, A. V. G., "Scattering of turbulent-jet wavepackets by a swept trailing edge," *The Journal of the Acoustical Society of America*, Vol. 140, No. 6, 2016, pp. 4350–4359. doi:10.1121/1.4971425.

[14] van der Velden, W. C. P., Casalino, D., Gopalakrishnan, P., Jammalamadaka, A., Li, Y., Zhang, R., and Chen, H., "Jet Noise Prediction : Validation and Physical Insight," *24th AIAA/CEAS Aeroacoustics Conference*, Atlanta, GA, USA, 2018, pp. 1–16.

[15] Brown, C., "Jet-Surface Interaction Test: Far-Field Noise Results," *Proceedings of the ASME Turbo Expo 2012: Power for Land, Sea and Air*, Copenhagen, Denmark, 2012, pp. 1–13.

[16] Podboy, G. G., "Jet-Surface Interaction Test: Phased Array Noise Source Localization Results," *NASA/TM—2013-218085*, 2013. doi:10.1115/GT2012-69801.

[17] Lew, P., Mongeau, L., and Lyrintzis, A., "Noise prediction of a subsonic turbulent round jet using the lattice-Boltzmann method," *The Journal of the Acoustical Society of America*, Vol. 128, No. 3, 2010, p. 1118. doi:10.1121/1.3458846.

[18] Brès, G., Pérot, F., and Freed, D., "Properties of the Lattice Boltzmann Method for Acoustics," *15th AIAA/CEAS Aeroacoustics Conference (30th AIAA Aeroacoustics Conference)*, 2009. doi:10.2514/6.2009-3395.

[19] Ffowcs-Williams, J. E., and Hawkings, D. L., "Sound Generation by Turbulence and Surfaces in Arbitrary Motion," *Philosophical Transactions of the Royal Society A: Mathematical, Physical and Engineering Sciences*, 1969. doi:10.1098/rsta.1969.0031.

[20] Farassat, F., and Succi, G. P., "A review of propeller discrete frequency noise prediction technology with emphasis on two current methods for time domain calculations," *Journal of Sound and Vibration*, Vol. 71, No. 3, 1980, pp. 399–419. doi:10.1016/0022-460X(80)90422-8.

[21] Casalino, D., "An advanced time approach for acoustic analogy predictions," *Journal of Sound and Vibration*, 2003. doi:10.1016/S0022-460X(02)00986-0.

[22] da Silva, F. D., Deschamps, C. J., da Silva, A. R., and Simões, L. G. C., "Assessment of Jet-Plate Interaction Noise Using the Lattice Boltzmann Method," *21st AIAA/CEAS Aeroacoustics Conference*, Dallas, TX, 2015. doi:10.2514/6.2015-2207.

[23] Casalino, D., Hazir, A., and Mann, A., "Turbofan Broadband Noise Prediction Using the Lattice Boltzmann Method," *AIAA Journal*, 2017. doi:10.2514/1.J055674.

[24] Casalino, D., Avallone, F., Gonzalez-Martino, I., and Ragni, D., "Aeroacoustic study of a wavy stator leading edge in a realistic fan/OGV stage," *Journal of Sound and Vibration*, Vol. 442, 2019, pp. 138–154. doi:10.1016/j.jsv.2018.10.057, URL https://doi.org/10.1016/j.jsv.2018.10.057.

[25] Gonzalez-Martino, I., and Casalino, D., "Fan Tonal and Broadband Noise Simulations at Transonic Operating Conditions Using Lattice-Boltzmann Methods," *2018 AIAA/CEAS Aeroacoustics Conference*, 2018. doi:10.2514/6.2018-3919.

[26] Bres, G. A., Nichols, J. W., Lele, S. K., and Ham, F. E., "Towards Best Practices for Jet Noise Predictions with Unstructured Large Eddy Simulations," *42nd AIAA Fluid Dynamics Conference and Exhibit*, New Orleans, LA, USA, 2012.

[27] Colonius, T., Lele, S. K., and Moin, P., "Sound generation in a mixing layer," *Journal of Fluid Mechanics*, 1997. doi:10.1017/S0022112096003928.

[28] Bridges, J., and Wernet, M., "Establishing Consensus Turbulence Statistics for Hot Subsonic Jets," *16th AIAA/CEAS Aeroacoustics Conference*, , No. June, 2010, pp. 1–41. doi:10.2514/6.2010-3751.

[29] Brown, C., and Wernet, M., "Jet-Surface Interaction Test: Flow Measurement Results," *20th AIAA/CEAS Aeroacoustics Conference*, Atlanta, GA, USA, 2014. doi:10.2514/6.2014-3198.

[30] Arndt, R. E. A., Long, D. F., and Glauser, M. N., "The proper orthogonal decomposition of pressure fluctuations surrounding a turbulent jet," *Journal of Fluid Mechanics*, Vol. 340, 1997, pp. 1–33. doi:10.1017/S0022112097005089.

[31] Lighthill, M. J., "On Sound Generated Aerodynamically I. General Theory," *Proceedings of the Royal Society A: Mathematical, Physical and Engineering Sciences*, 1952. doi:10.1098/rspa.1952.0060.

[32] Jordan, P., and Colonius, T., "Wave Packets and Turbulent Jet Noise," *Annual Review of Fluid Mechanics*, 2013. doi:10.1146/annurev-fluid-011212-140756.